Photocatalytic Degradation of o-Chloranil on Nano Crystalline Cellulose Doped Titania

Moodley V.,* Maddıla S., Jonnalagadda S.B. And Van Zyl W.E

[1] School of Chemistry and Physic, University of KwaZulu-Natal, Westville campus, Westville, Durban, 4000, South Africa

*corresponding author: Vashen Moodley

e-mail: 210545761@stu.ukzn.ac.za

Abstract. The photocatalytic degradation of *o*-chloranil was investigated in aqueous mixtures of nanocrystalline cellulose (NCC) doped titanium dioxide. Different loadings of catalysts NCC/TiO_2 (10, 20, 40 and 80%) was synthesized and characterized by analytical techniques. The degradation was examined by observing the variation in substrate concentration employing UV spectroscopic analysis as a function of irradiation time in the presence of UV light at neutral pH condition. The 20% NCC/TiO_2 catalyst showed excellent degradation and mineralization of *o*-chloranil in 2 h. The degradation products were analysed and identified by using LC-MS. The photo-catalyst offers many benefits such as easy preparation, non-hazardous, inexpensive, high stability and recyclability with no loss of activity.

Keywords: *o*-Chloranil; Advanced Oxidation Process; Nano Crystalline Cellulose; TiO_2; Photocatalytic Degradation.

1. Introduction

Environmental pollution is one of the major and uncontrolled hazards of the modern world (William *et al.*, 2003). Progress in agricultural, medicinal, and alternative energy areas are necessary in order to attain the needs and demands of an ever growing anthropological population (Michael 1991). Greener processes are required for the creation of environmentally friendly products. The focus should be shifted to the eradication and reduction of existing environmental pollutants and move toward a sustainable society where green chemistry processes and environmental remediation are necessary (Joseph 2003).

There has been a remarkable increase in awareness of the toxic and carcinogenic effects of many polluting chemicals that were not considered hazardous only two decades ago (Ibrahim 1997). One such pollutant has been identified as *o*-chloranil (2,3,5,6-tetrachloro-2,5-cyclohexadiene-1,4-dione), which was observed as an oxidation by-product of pentachlorophenol (PCP) (Ricotta *et al*., 1996). In the past, *o*-chloranil was used as a fungicide and algicide under the trade name Spergon (Armin 1995). Control of organic pollutants in water sources is an important measure in environmental protection. Biodegradation pathways have garnered great attention amongst the proposed and developed processes for the elimination of organic contaminants.

In recent years, photo-catalysis has gained advancement in current research endeavours due to its economical and green synthetic route, which incorporates advanced oxidation processes (AOP) for removal of organic impurities (Maddila *et al*., 2015a). During AOP, an illuminated semiconductor absorbs light and generates active species such as hydroxyl radicals, holes and superoxide anions (Oseghe *et al*., 2015). The use of titania is diminished by its wide bandgap (3.2 eV), which requires ultraviolet irradiation (λ < 387 nm) for photocatalytic activation to inject electrons into the conduction band and leave holes in the valence band (Maddila *et al*., 2015b). To aid the reaction of titania, by enhancing the separation of electron–hole pairs, reducing electron–hole recombination rates and increase the photocatalytic efficiency, titania is typically doped with support. This method has proven to show high chemical stability, non-toxicity, low concentrations and low cost as well as achieve a comprehensive degradation and mineralization (Maddila *et al*., 2015a, 2015b, 2016a; Oseghe 2015).

Cellulose is the most abundant biopolymer in the world, with wide-scale potential growth. The end product of Nano Crystalline Cellulose (NCC), is a highly tailored material with enhanced mechanical, physical and optical properties (Habibi *et al.*, 2010; Peng *et al*., 2011; Klemm *et al*., 2011). The material is produced through chemical, mechanical or biological modification of cellulose to achieve the desired NCC with lengths ranging from 50–200 nm and widths from 5–20 nm (Eyley and Thielemans, 2014). Due to its potential photonic use as a chiral nematic material, which leads to iridescent coloured films, NCC was chosen as a second phase in the nanocomposite (Kelly *et al.*, 2014; Zhou *et al.*, 2013). Chiral nematic NCC could act as a potential charge carrier, and in turn increase the efficiency of TiO_2 as a photocatalyst by lowering the rate of electron recombination. Thus a nanocomposite of (NCC/TiO_2) could be used for photocatalytic decomposition of organic pollutants. In this work, we demonstrate the facile fabrication of an NCC/TiO_2 nanocomposite hybrid by the adsorption of TiO_2 (anatase) nanoparticles on wood-derived nano-fibrillated cellulose as well as the use of this hybrid in the photocatalytic degradation of *o*-chloranil.

2. Materials and Method

2.1 Photocatalytic study

The photodegradation of *o*-chloranil with a fixed absorbance of 0.3281 at a λ_{max} of 298 nm was undertaken. The light source was sunlight to imitate real-world conditions (26°C and clear day). A 2L, 10 ppm solution of *o*-chloranil was prepared and further sonicated for 10 mins to allow total dissolution of o-chloranil. Afterwards, 250 mL of the *o*-chloranil solution was added to an 800 mL beaker containing 200 mg of catalyst (Control, bare TiO_2, NCC/TiO_2 (10%, 20%, 40% and 80% w/w%) and pure NCC). Initial absorbance measurements were taken 60 min prior to investigation in a darkroom with set-up moved to the reaction site in darkness conditions. The reaction was stirred for 120 min with absorbance measurements taken every 20 mins.

2.2. Catalyst preparation

The NCC was prepared by dissolving (hardwood) pulp using a sulfuric acid (65% w/w) hydrolysis treatment. Dissolving pulp (5.0 g) was mixed with 100 mL of sulfuric acid solution, and the mixture was stirred vigorously (700 rpm) at 64°C for 1 hour. The mixture was diluted 10-fold with deionized water to stop the hydrolysis reaction and the diluted mixture was then centrifuged at 9000 rpm for 15 min to concentrate the cellulose and remove excess acid. The precipitated material was rinsed with distilled water and centrifuged again, this process was repeated 3 times and then dialyzed in dialysis sacks, with an average flat width 25 mm, MWCO 12,000 Da, against deionized water for one week until a pH of 7 was reached. The dialyzed nanocellulose was sonicated for 5 min with cooling in an ice bath at 75 % output and 0.7 cycles to obtain the NCC colloidal solution.

The photocatalysts were prepared by the deposition-precipitation method by impregnating NCC over titania. TiO_2 (0.9, 0.8, 0.6, 0.2 g) was suspended in 50 mL of deionized water with vigorous stirring for 30 min. Then, NCC (prepared, 0.1, 0.2, 0.4, 0.8 g) was added with additional stirring for 1.0 h. Thereafter, the pH was adjusted to 8.5 using 0.1 M NaOH solution. The suspension was vigorously stirred for a further 2 h. The precipitates were heated at 60-70 °C for 2 h in solution. The precipitates were then sonicated, filtered and washed with deionized water. The samples were dried at 90-100°C overnight to obtain the 10%, 20%, 40, and 80% w/w% of NCC/TiO_2 catalysts.

2.3. Instrumentation

All the catalyst characterization and product identification were achieved adopting the following techniques: PXRD, SEM-EDX, TEM, N_2 sorption, ICP, PL, FTIR and GC-MS (Maddila *et al*., 2016a & b).

3. Results and Discussion

3.1. BET surface and elemental analysis

The N_2 sorption study was carried out over bare TiO_2 and NCC doped TiO_2 catalysts (**Figure. 1**). N_2 sorption resulted in typical type V isotherm, with a narrow H_2 hysteresis loop.

Table 1. Surface area and pore volumes of synthesized catalysts.

Catalyst	Surface area m^2/g	Pore Volume cm^3/g
Pure Titania	8.5804	0.104178
10% NCC/Titania	10.617	0.04967
20% NCC/Titania	10.0752	0.059678
40% NCC/Titania	10.5717	0.069155
80% NCC/Titania	1.9559	0.029933

The BET surface areas of bare TiO_2, 10%, 20 %, 40 %, and 80% NCC/TiO_2 catalysts were found to be 8.58, 10.617, 10.075, 10.572, 1.956 $m^2.g^{-1}$, respectively. It is evident from these results that there was a significant change in the surface area from the TiO_2 to NCC doped TiO_2 catalyst. We see a drastic decrease in surface area and pore volume as the NCC dopant increases (**Table 1**).

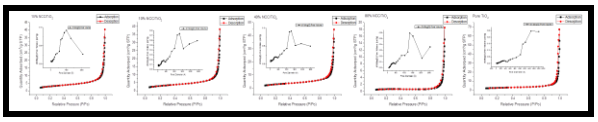

Figure 1. N_2 adsorption-desorption isotherm plots of synthesized catalysts with pore volume density (insets)

3.2. SEM and TEM

The transition electron microscopy (TEM) micrographs of bare TiO_2 (Figure 2i) showed disc-shaped particles with sizes ranging between 100 – 200 nm in length. The size of TiO_2 particles deposited on the NCC catalysts showed no significant changes when compared to the neat TiO_2 particles, however, strand/bone like NCC particles are evident upon staining of samples (Figure 2b, 2d, 2f and 2h). Sizes of NCC particles range between 100 – 400 nm in length which coincides with NCC parameters (Figure 2j). With the introduction of NCC into the TiO_2 matrix, the spherical particles appeared to have aggregated, forming clusters and colonizing the NCC particles.

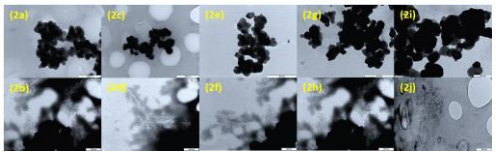

Figure 2. TEM micrographs of unstained and stained 10% (2a-2b), 20% (2c-2d), 40% (2e-2f) and 80% (2g-2h) NCC/TiO_2 catalysts. Bare TiO_2 (2i) and NCC (2j) are shown.

The particles are large with elliptical irregular shapes which are perceived from the high magnification SEM micrograph (**Figure 3**). The micrographs show that the TiO_2 particles are in an aggregative state and adhere onto NCC rods. A homogeneous distribution of smaller TiO_2 particles is seen on the surface of larger TiO_2 particles (Figure 3g-h). This is quantified by the EDS mapping (Figure 3i). Furthermore, the morphology of the catalyst points to a semi-crystalline and homogenous sample.

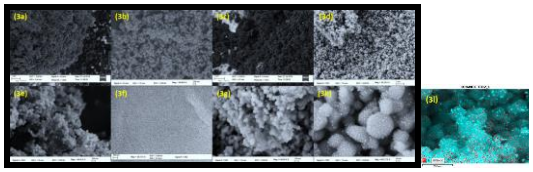

Figure 3. SEM micrographs of 10%, 20%, 40% and 80% (3a-d) NCC/TiO_2 catalysts. Bare TiO_2 (3e) and NCC (3f). Magnification (3g-3h) and SEM-EDS mapping (3i) of 20% NCC/TiO_2.

3.3. XRD analysis

The prepared catalysts show the presence of the TiO_2 anatase phases. The diffraction peaks located at 2θ = 25.2°, 37.9°, 48.0° and 62.0° are indexed to (101), (004), (200) and (204) planes of anatase phase TiO_2 (Luo *et al*., 2013). The phases of TiO_2 correlate with that of literature (Chetty *et al*., 2012). The increase in the NCC loading was shown by slight peak shift in the XRD diffractogram at 2θ = 13° and 23°.

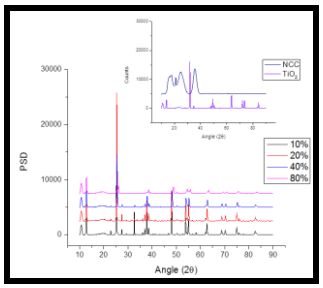

Figure 4. The PXRD pattern of (inset) pure NCC Bare TiO_2 (anatase), 10%, 20%, 40% and 80% NCC–TiO_2.

By increasing in NCC loading, there is no evidence of an additional phase of NCC.

3.4. UV-diffuse reflectance spectra

The dense absorption band at nearly 372 nm conform to a band-gap energy of 3.21 eV calculated from the formula k = 1239.8/Ebg. On doping with NCC, a red-shift was detected which could foster the photocatalytic activities of the catalyst under visible light.

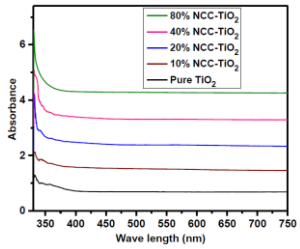

Figure 5. UV-DRS of bare TiO_2 and synthesized (% w/w) NCC doped TiO_2 catalysts

3.5. Photoluminescence spectra

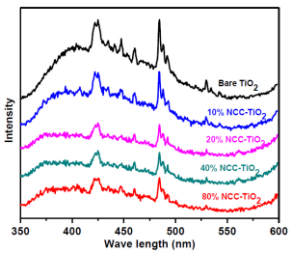

Figure 6. Photoluminescence spectra of bare TiO_2 and synthesized (% w/w) NCC doped TiO_2 catalysts

The PL spectra of NCC/TiO_2 samples range between 350–500 nm with an excitation wavelength of 360 nm. The PL spectra might be closely related to the recombination of photoinduced electrons and holes, and free and self-trapped excitons, which possibly generate from surface defects in the TiO_2 crystals, such as lattice distortions and surface oxygen deficiencies. The spectra illustrates that with the increase of NCC loading, a decrease in intensity is seen. This indicates the reduction of the recombination centers for the electrons and holes in the samples. This suggests that the NCC/TiO_2 catalysts lead to low rates of electron-holes recombination under light irradiation and may show better photocatalytic activity than bare TiO_2.

3.7. Catalyst loading concentration

The photocatalyst loading was increased from 50 mg/L to 200 mg/L (**Figure 7**). From the experiments, the 100 mg/L catalyst was the most efficient for *o*-chloranil photo-degradation. When the catalyst concentration increases, the reaction rate decreases. This may be due to the accessibility of sufficient catalytic active sites on the catalyst material surface and also the penetration of light into the suspension.

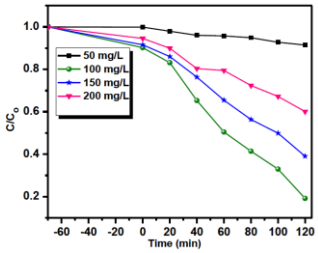

Figure 7. Influence of the amount of catalyst loading on the *o*-chloranil photo-degradation

3.8. Degradation of o-chloranil

Figure 8 shows degradation of o-chloranil as a function of time using different catalyst materials and also Degussa P25 under visible light, after equilibrating in the dark for 60 min. The catalyst material of NCC/TiO_2 with 20% NCC doping displays the highest photocatalytic activity due to the ability of nanocellulose assisting in the seizure of electrons to achieve a higher photocatalytic activity with a suitable doping concentration.

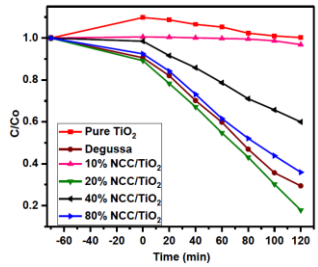

Figure 8. The photo-degradation *o*-chloranil as a function of time

With the increase in the concentration of cellulose doping, the recombination of photogenerated electron-hole pairs may result, leading to a decrease in the photocatalytic activity. Therefore, a higher loading of NCC > 20 wt% was required.

3.9. *Identification of products*

All the photocatalyzed investigations were accompanied by exposing the reaction mixture to visible light. The organic portion of the reaction mixture was extracted and analyzed after every reaction with 20 min intervals. Three products were identified by gas chromatography (GC) (**Figure. 9a**).

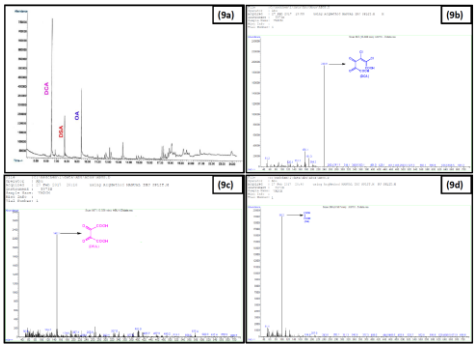

Figure 9. Degradation products confirmed by Chromatogram (9a) and LC mass spectra of degradation products (9b, 9c and 9d)

The peaks at retention times 15.807 (**Figure 9b**), 13.558 (**Figure 9c**) and 8.507 (**Figure 9d**) minutes refer to the compounds of 2,3-dichloro-4,5-dioxohex-2-enedoic acid (DCA), 2,3-dioxosuccinic acid (DSA) and oxalic acid (OA), respectively. Furthermore, the formation of these products were confirmed by LC-MS with their respective (M^+) m/z values.

3.10. *Reaction mechanism*

Based on the aforementioned results, a possible reaction mechanism (**Scheme 1**) for the photocatalytic degradation of *o*-chloranil is proposed.

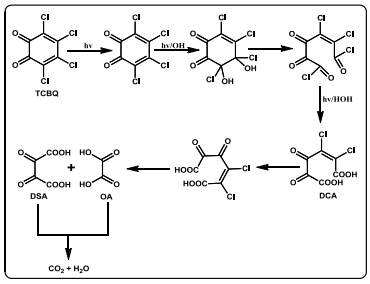

Scheme 1. The proposed mechanism for the photo-degradation *o*-chloranil.

In aromatic substituted compound, chloro functional groups are electron withdrawing groups; the hydroxyl radical (˙OH) attack leads to the elimination of chlorides to form a ring open molecule. This leads to the transformation to the aliphatic acid, via further attack by ˙OH. The short-lived intermediate, DCA, favours the electrophilic substitution of ˙OH at the supplementary chloro position, and forms a dechlorinated species through photo-oxidation. The further oxidation of the intermediate by ˙OH, leads to oxygenated aliphatic compounds and formation of degraded aliphatic carboxylic acids. Two aliphatic acids (DSA and OA) were identified in this study. Further oxidation of these acid products leads to complete mineralization to CO_2 and H_2O.

3.11 *Conclusions*

NCC doped TiO_2 can efficiently catalyze the photodegradation and mineralization of the pollutant *o*-chloranil in the presence of light. The results show that rate of degradation can be influenced not only by the various parameters, such as substrate concentration and photocatalyst loading, but also by an ideal pollutant. The slow mineralization of the source pollutant can be attributed to the intermediate formed. This provides a useful source of information for the degradation pathways. Our investigation suggests that DCA, DSA and OA are the main intermediates formed during the photo degradation of the model contaminant.

4. **Acknowledgements**

The authors are grateful to the National Research Foundation of South Africa for funding and the University of KwaZulu-Natal for providing the environment necessary to facilitate this work.

References

Armin B. (1995). Dioxins and related compounds. *Environ. Sci. & Pollu. Res*. **2(2)**, 117–121.

Chetty E. C., Dasireddy V. B., Maddila S., Jonnalagadda S. B. (2012) Efficient conversion of 1,2-dichlorobenzene to mucochloric acid with ozonation catalyzed by V_2O_5 loaded metal oxides. *Applied Catalysis B: Environmental.* **117–118**, 18-28.

Eyley S. and Thielemans W. (2014). Surface modification of cellulose nanocrystals *Nanoscale*, **6**, 7764-7779.

Habibi Y., Lucia L.A. and Rojas, O.J. (2010). Cellulose nanocrystals: Chemistry, self-assembly, and applications. *Chem. Rev.* **110**, 3479-3500.

Ibrahim D. (1997). Energy and environmental impacts: Present and future perspectives. *J. Energ. Sour*., **20(4-5)**, 427-453.

Joseph F. (2003). Designing resilient, sustainable systems. *Environ. Sci. Technol.*, ***37*(23)**, 5330–5339.

Kelly J.A., Giese M., Shopsowitz K.E., Hamad W.Y. and MacLachlan M.J. (2014). The development of chiral nematic mesoporous materials. *Acc. Chem. Res. 47*, 1088−1096.

Klemm D., Kramer F., Moritz S., Lindström T., Ankerfors M., Gray D. and Dorris A. (2011). Nanocelluloses: A new family of nature-based materials. *Angewan. Chem. Internat. Edi.* **50**, 5438-5466.

Luo Y., Liu X., Huang J. (2013) Heterogeneous nanotubular anatase/rutile titania composite derived from natural cellulose substance and its photocatalytic property. *CrystEngComm.* **15**, 5586-5590.

Maddila S., Lavanya P. and Jonnalagadda S.B. (2015a). Degradation, mineralization of bromoxynil pesticide by heterogeneous photocatalytic ozonation. *J. Indu. & Eng. Chem.* **24,** 334-341.

Maddila S., Rana S., Pagadala R. and Jonnalagadda S.B. (2016). Photocatalysed ozonation: Effective degradation and mineralization of pesticide, chlorothalonil. *Desalinat. & Water Treatment*. **57**, 14506-14517.

Maddila S., Rana S., Pagadala R., Maddila S.N., Chandrasekhar V. and Jonnalagadda S.B. (2015b). Ozone driven photocatalyzed degradation and mineralization of pesticide, Triclopyr by Au/TiO_2. *J. Environ. Sci. & Heal. Part B,* **50,** 1-13.

Maddila S., Oseghe E.O. and Jonnalagadda S.B. (2016). Photocatalysed ozonation by Ce doped TiO2 catalyst degradation of pesticide, Dicamba in water. *J. Chem. Technol. & Biotechnol*. 91, 385-393.

Michael E.C. (1991). Environmental management in development: the evolution of paradigms. *Ecolog. Economic*., **3(3)**, 193-213.

Oseghe E.O., Maddila S. and Jonnalagadda S.B. (2015). Effect of surfactant concentration on active species generation and photocatalytic properties of TiO_2. *Appl. Catal. B: Environ*. **176-177**, 288-297.

Peng B.L., Dhar N., Liu H.L. and Tam K.C. (2011). Chemistry and applications of nanocrystalline cellulose and its derivatives: a nanotechnology perspective. *The Can. J. Chem. Eng*. **89**, 1191-1206.

Ricotta A., Unz R.F. and Bollag J-M. (1996). Role of a laccase in the degradation of pentachlorophenol. *Bull. Environ. Contamin. & Toxicol*., **57(4),** 560–567.

William A.S., Kerry M. and Maureen D.A. (2003) Environmental hazards to children's health in the modern world. *Mutation Res./Rev. in Mutat. Res.*, **544(2–3)**, 235–242.

Zhou Y., Fuentes-Hernandez C., Khan T.M., Liu J.C., Hsu J., Shim J.W., Dindar A., Youngblood J.P., Moon R.J. and Kippelen B. (2013). Recyclable organic solar cells on cellulose nanocrystal substrates. *Sci. Rep*. **3**, 1536-1540.